Journal of Applied Fluid Mechanics, Vol. 16, No. 8, pp. 1515-1530, 2023.
Available online at www.jafmonline.net, ISSN 1735-3572, EISSN 1735-3645.
https://doi.org/10.47176/jafm.16.08.1702

An Evaluation of Inflow Profiles for CFD Modeling of Neutral ABL and Turbulent Airflow over a Hill Model

N. Amahjour[1†], A. Sofi[2], J. R. Rodríguez Galván[3], A. El Kharrim[2] and A. Khamlichi[4]

[1]*Department of Physics, Faculty of Sciences, Abdelmalek Essaadi University, Tetouan, 93002, Morocco*
[2]*Team: Energy, materials, numerical physics, Higher Normal School, Abdelmalek Essaadi University, Tetouan,93100, Morocco*
[3] *Department of Mathematics, Faculty of Sciences, Cadiz University, Poligono Rio San Pedro S/N Puerto Real, Cadiz, 11510, Spain*
[4]*Department of STIC, National School of Applied Sciences, Abdelmalek Essaadi University, Tetouan, 93002, Morocco*

†*Corresponding Author Email: narjisse.amahjour@etu.uae.ac.ma*

ABSTRACT

The implementation of the wind turbine is a major issue in the wind engineering sector. However, the presence of wind turbines in the lower part of the atmospheric boundary layer (ABL) requires an appropriate study for the simulation of turbulent airflow in the wind farm situated on hilly terrain. The use of precise Computational Fluid Dynamics (CFD) simulations for the ABL flow is vital for numerous applications, such as wind energy, building, urban planning, etc. To achieve accurate results, it is imperative that the inlet boundary conditions produce vertical profiles that keep a uniform horizontal distribution (with no streamwise gradients) in the upstream region of the computational domain for all important parameters. A development approach is proposed herein, focused on the imposition of two different inlet profiles when used in combination with the rough z0-type scalable wall function. The horizontal homogeneity of these profiles has been verified by 2D Reynolds averaged Navier-Stokes (RANS) through the examination of a neutral ABL in an empty computational domain using the k-ε turbulence model. The findings indicate that the use of this modeling approach can yield relatively consistent homogeneity of neutral ABL for both inlet boundary conditions. Subsequently, sensitivity analyses were performed on the inflow profiles to forecast the evolution of the bottom half of an idealized truly-neutral ABL and to accurately capture the complex dynamics of atmospheric flows over hilly terrain. This study compares the results with the CRIACIV (Inter-University Research Centre on Building Aerodynamics and Wind Engineering) boundary layer wind tunnel experimental data, showing that the inflow profiles and the presence of topographic complex have a significant impact on air velocity, turbulent kinetic energy and turbulence intensity in the x-direction. The results obtained are in good correlation with published experimental data in the presence of the hill surface.

Article History

Received December 8, 2022
Revised April 1, 2023
Accepted April 3, 2023
Available online May 31, 2023

Keywords

Computational wind engineering
k-ε turbulence model
Neutral Atmospheric Boundary Layer (ABL)
Horizontal homogeneity
Roughness surface
FEM
Hill

1. INTRODUCTION

The accuracy of wind turbines is heavily dependent on their positions in wind farms. Wind turbines must be installed in areas with high winds in order to attain a significant amount of wind energy potential. The airflow over complex terrain, such as hills, mountains, and valleys, is characterized by significant turbulence, separation, and recirculation, which can affect the performance and safety of wind energy systems. For this reason, several researchers have studied the airflow around hills, given the acceleration that is created on the top of the hill (Lubitz & White, 2007; Narjisse & Abdellatif, 2021; Yang et al., 2021; Zheng & Tian, 2018).

Numerical models based on Reynolds-averaged Navier-Stokes (RANS) equations are widely used to simulate the ABL and airflow over complex terrain, as they offer a balance between accuracy and computational efficiency. However, the accuracy of RANS simulations depends on the accuracy of the inflow boundary conditions, which are used to specify the velocity, turbulence, and other flow parameters at the domain inlet. Inaccurate inflow boundary conditions can lead to incorrect predictions of the flow field, such as underestimation or overestimation of turbulence, wake effects, and power output of wind turbines.

Nomenclature

Parameters

C_s	roughness constant
E	integration constant
H	height of the hill
h^+	dimensionless height of the first mesh cell
k	turbulent kinetic energy
k_s	equivalent sand grain roughness height
k_s^+	dimensionless of equivalent sand grain roughness height
L	half distance of the hill
p	pressure
R_e	Reynolds number
R_k & R_k	Residuals
U_{ref}	mean velocity at the hill-model height
S_φ	sources terms
u_*	friction velocity
u_j	velocity vector
$u_i^{'}, u_j^{'}, w^{'}$	fluctuating velocity components
x_j	cartesian coordinate
z_0	roughness length

Greek symbols

κ	Von Karman's constant
$C_\mu, C_{\varepsilon 1}, C_{\varepsilon 2}, \sigma_k$	closure constants
μ	dynamic viscosity
μ_t	turbulent dynamic viscosity
ρ	fluid density
ε	turbulent dissipation energy
τ_{ij}	shear stress
δ_w	distance from the wall
δ_w^+	dimensionless distance from the wall
δ_{ij}	Kronecker function

Abbreviations

ABL	Atmospheric Boundary Layer
BLWT	Boundary Layer Wind Tunnel
CFD	Computational Fluid Dynamics
CRIACIV	Centro di Ricerca Interuniversitario di Aerodinamica delle Ingegneria del Vento – Inter-University Research Centre on Building Aerodynamics and Wind Engineering
ESDU	Engineering Science Data Unit
FEM	Finite Element Method
RANS	Reynolds averaged Navier-Stokes
RH	Richards and Hoxey
UDE	User Defined Function

The challenge is to obtain an accurate numerical simulation of the atmospheric boundary layer (ABL), which remains one of the requirements in different engineering applications. For several years, much effort has been devoted to examining and investigating the complexity involved in simulating an equilibrium ABL with RANS specifically, on the neutral ABL condition, where the buoyancy force is negligible, and the flow is dominated by the wind shear. (see, for example (Blocken et al., 2007a; Yang et al., 2008; Parente et al., 2010, 2011; Yang et al., 2017; Tian et al., 2018). In general, two significant factors should be taken into consideration.

One important step in this process is to simulate horizontally homogenous ABL flows, since the lower part of ABL plays an important role in wind engineering because that is where the wind turbines operate. If there are no streamwise gradients in mean wind speed or turbulent amounts, the simulated wind flows can be considered horizontally homogeneous (Yan et al., 2015). Maintaining a horizontally uniform atmospheric boundary layer is crucial because it ensures that the wind profiles applied to the complex terrain are consistent with those provided by the modeler. Much research in this field has shown that it is difficult to simulate the horizontally homogeneous flow (Richards & Hoxey, 1993; Blocken et al., 2007b; Hargreaves & Wright, 2007; Yang et al., 2009; Norris & Richards, 2010; Tian et al., 2018), which may be related to inconsistencies in turbulence model, inlet and wall function conditions. Many researchers have discovered inaccuracies due to inconsistencies in the upper boundary conditions, emphasizing the necessity of turbulence model closure parameters (Richards & Hoxey, 1993; Yang et al., 2009; Norris & Richards, 2010). Nevertheless, based on inaccurate streamwise gradients in the recommended profiles, it has been noted that the typical use of two equation RANS models with the standard wall function may give rise to inappropriate predictions. Blocken et al. (2007a) have indicated that the main source of the ABL inhomogeneity problem is due to the inconsistent limits to the standard wall function in different commercial Computational Fluid Dynamics (CFD) codes, since they are based on mesh consequences close to the ground surface during the numerical simulation of the boundary layer, which entails the instability of the computational and the difficulty of achieving the ABL homogeneity. Parente et al. (Parente et al., 2011) solved

this major problem for the turbulence model by improving the near-wall condition, proposing a novel wall function with roughness based on aerodynamic roughness length (z_0).

In order to gain some insight into how to appropriately describe the ABL flow, Richard and Hoxey (Richards & Hoxey, 1993; Norris & Richards, 2010) fulfilled the requirements for modeling the horizontal homogeneous atmospheric boundary layer by using RANS simulations. They calculated the necessary boundary conditions for achieving the consistency of the developed profiles in ABL by using a constant shear stress assumption with the conjunction of the turbulence model.

The studies addressing the ABL inhomogeneity problem have largely concentrated on the improvement of modeling, with the aim of decreasing the ABL inhomogeneity while obtaining accurate inlet boundary conditions and exact turbulence modeling (Pontiggia et al., 2009; Yang et al., 2009; Juretic & Kozmar, 2013; Parente et al., 2017; Abu-Zidan et al., 2020b).

When it comes to turbulent airflow over a hill model, the complexity of the flow field poses additional challenges to the specification of inflow boundary conditions. In particular, the turbulence generated by the hill can significantly affect by the inflow conditions, making it difficult to obtain accurate and consistent results. Recent literature has investigated the impact of different inflow boundary conditions on the accuracy and reliability of CFD simulations. For example, (Abu-Zidan et al., 2020a) investigated the impact of ABL inhomogeneity on the accuracy of CFD simulation of wind loading around tall buildings. The study found that the inhomogeneity of ABL has a significant impact on the accuracy of CFD simulations of tall buildings. The presence of ABL inhomogeneity can result in errors in predicted wind speeds, wind directions, and turbulence intensities. The authors suggest that accurate representation of ABL inhomogeneity in CFD simulations is essential for reliable of wind load predictions around tall buildings.

Tian et al. (2017) studied the accuracy of various inflow boundary conditions for RANS simulations of wind turbine wake flow and neutral ABL. The authors mentioned that the accuracy of RANS simulations of wind turbine wake flow and neutral ABL is highly dependent on the inflow boundary conditions used.

While several studies have managed to maintain the horizontal homogeneity in RANS simulations of simplified neutral ABLs over a uniformly rough surface by ensuring the remedial measures to the standard rough wall function, little attention has been paid to examining and exploring the impact of ABL consistency on wind speed predictions and intensity turbulent over a hill model by making the remedial measures to the scalable rough wall function. In summary, accurate specification of inflow boundary conditions is critical for obtaining reliable results in RANS simulations of neutral ABL and turbulent airflow over a hill model. While several methods and approaches have been proposed, there is still a need for further research to develop more robust and practical inflow boundary conditions for these types of simulations.

Therefore, the aim of this research is to provide insights into the strengths and weaknesses of different inflow boundary conditions such as RH profile and ESDU profile for RANS simulations of neutral ABL and airflow over a hill model, using both numerical and experimental data.

This article includes two complementary investigations, one dedicated to studying the performance of two different inflow conditions with the combination of developing a rough z0- type scalable wall function through a flat terrain (empty domain). The development condition was implemented in COMSOL software by User-Defined Equation (UDE). This modeling methodology enables the horizontal homogeneity of neutral ABL to be achieved, with the aim of assessing the accuracy of CFD simulation by using COMSOL based on the Finite Element Method (FEM) (Singh & Badodkar, 2016). In addition, in this first section the distribution of velocity and turbulence parameter profiles are presented, while the second consists in using the modeling methodology generated in the first investigation to examine the sensitivity of the inflow profiles on the evolution of airflow in a neutral Atmospheric boundary layer around the hill model. The study employs computational fluid dynamics (CFD) simulations to investigate the airflow over hilly terrain, and provide a detailed insight into the airflow characteristics, such as velocity profiles, turbulence kinetic energy and turbulence intensity, which is a complex and challenging problem. The configuration of the computational domain and hill were schematized on the basis of the characteristic measures of the CRIACIV boundary layer wind tunnel experiment data (Kozmar et al., 2018). Validation with data based on the prototype of the full-scale conditions is among the aims of this work.

The results of the study can help improve the accuracy and reliability of RANS simulations of the ABL and complex terrain flows, and support the design and optimization of wind energy systems and other applications.

This paper is divided into 6 Sections: Section 2 examines the theoretical background and introduces the methodology to achieve ABL homogeneity, including the appropriate corrective measures and a modified near-wall treatment. Afterward, Section 3 presents the details of the CRIACIV boundary layer wind tunnel (BLWT) data and the numerical setup. The profiles obtained for the horizontal homogenous ABL flow in an empty domain are described in Section 4. Section 5 presents the CFD simulation results and discussions concerning the performance of turbulent wind flow over a hill model from a wind energy perspective, and are validated to the CRIACIV experimental data. The conclusions and suggestions are outlined in Section 6.

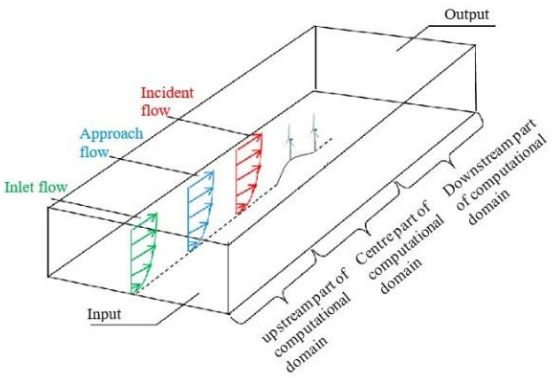

Fig. 1. Presentation of various part in CFD numerical simulation of ABL airflow in a wind farm situated on hilly terrain.

2. THEORETICAL BACKGROUND

2.1 Fluid Dynamics and Turbulence Model Equations

The governing RANS mathematical equations, conservation of mass, and momentum are primarily given by the equations below in the case of the incompressible, 2D steady state, coupled by the standard k-ε transport equations. This turbulence model and its family have been the most dominant and extensively employed models in wind engineering applications.

$$\frac{\partial \overline{u_j}}{\partial x_j} = 0 \tag{1}$$

$$\rho\left(\frac{\partial \overline{u_i}}{\partial t} + \overline{u_j}\frac{\partial \overline{u_i}}{\partial x_j}\right) = -\frac{\partial \overline{p}}{\partial x_i} + \frac{\partial}{\partial x_j}\left(\mu\left(\frac{\partial \overline{u_i}}{\partial x_j} + \frac{\partial \overline{u_j}}{\partial x_i}\right) - \overline{\rho u_i' u_j'}\right) \tag{2}$$

where ρ is the fluid density, $\overline{u_j}$ is the velocity vector, $\overline{u}$ the averaged velocity vector field, p the mean fluid pressure, and μ is the dynamic viscosity, which depends exclusively on the material properties. The term on the right side of the momentum Eq. (2) refers to the Reynolds stress term $-\rho\overline{u_i' u_j'}$, which should be determined by the average flow values. Regarding the Boussinesq approximation, which relates the shear stress and the average velocity gradients by the turbulent eddy viscosity μ_t, this term can be expressed by the following formulation:

$$\tau_{ij} = -\rho\overline{u_i' u_j'} = \mu_t\left(\frac{\partial \overline{u_i}}{\partial x_j} + \frac{\partial \overline{u_j}}{\partial x_i}\right) - \frac{2}{3}\rho k \delta_{ij} \tag{3}$$

where:

$$\mu_t = C_\mu \rho \frac{k^2}{\varepsilon} \tag{4}$$

δ_{ij} is the Kronecker function and $k = \frac{1}{2}\overline{u_i' u_i'}$ is the turbulent kinetic energy.

$$\rho\frac{\partial k}{\partial t} + \rho\overline{u_i}\frac{\partial k}{\partial x_j} = \frac{\partial}{\partial x_i}\left[\left(\mu + \frac{\mu_t}{\sigma_k}\right)\frac{\partial k}{\partial x_i}\right] + P_k - \rho\varepsilon + S_k \tag{5}$$

$$\rho\frac{\partial \varepsilon}{\partial t} + \rho\overline{u_i}\frac{\partial \varepsilon}{\partial x_j} = \frac{\partial}{\partial x_i}\left[\left(\mu + \frac{\mu_t}{\sigma_\varepsilon}\right)\frac{\partial \varepsilon}{\partial x_i}\right] + C_{\varepsilon 1}\frac{\varepsilon}{k}P_k - C_{\varepsilon 2}\rho\frac{\varepsilon^2}{k} + S_\varepsilon \tag{6}$$

S_k, S_ε defines the sources/sinks terms, k and ε are the turbulence kinetic energy and dissipation energy, respectively, while P_k refers to the production of the turbulent kinetic energy term and can be expressed by Eq. (7):

$$P_k = \mu_t\left(\frac{\partial \overline{u_i}}{\partial x_j} + \frac{\partial \overline{u_j}}{\partial x_i}\right)\frac{\partial \overline{u_i}}{\partial x_j} \tag{7}$$

$C_\mu, C_{\varepsilon 1}, C_{\varepsilon 2}, \sigma_k, \sigma_\varepsilon$ are the closure constants of the $k-\varepsilon$ turbulence model, and κ is von Karman constant. The corresponding values of these parameters are summarized in Table 1:

Table 1 Standard values of the closure constants for the $k-\varepsilon$ model.

Closure constant	C_μ	$C_{\varepsilon 1}$	$C_{\varepsilon 2}$	σ_k	σ_ε	κ
Standard	0.09	1.44	1.92	1.0	1.3	0.41

2.2 Mathematical Equations of Neutral Horizontally Homogeneous ABL Flow

In the case study of a neutral condition of the ABL, the variation of air velocity and turbulence parameters is a function only of the height above the surface (Z), because it is regarded as a horizontally homogeneous turbulence layer. So, Eq. (7) can be expressed in the following manner:

$$P_k = \mu_t\left(\frac{\partial u}{\partial z}\right)^2 \tag{8}$$

The governing equation describing the case of two-dimensional ABL flow coupled with the $k-\varepsilon$ closure model, based on the hypothesis of constant pressure in the vertical velocity, stream-wise directions, constant shear stress, and also in the highly turbulent flows $\mu_t \gg \mu$, are reduced to:

$$\mu_t\left(\frac{\partial u}{\partial z}\right) = \tau_w = \rho\left(-\overline{u'w'}\right) \tag{9}$$

$$\frac{\partial}{\partial z}\left(\frac{\mu_t}{\sigma_k}\frac{\partial k}{\partial z}\right) + \mu_t\left(\frac{\partial u}{\partial z}\right)^2 - \rho\varepsilon + S_k = 0 \tag{10}$$

$$\frac{\partial}{\partial z}\left(\frac{\mu_t}{\sigma_\varepsilon}\frac{\partial \varepsilon}{\partial z}\right)+C_{\varepsilon 1}\frac{\varepsilon}{k}\mu_t\left(\frac{\partial u}{\partial z}\right)^2-C_{\varepsilon 2}\rho\frac{\varepsilon^2}{k}+S_\varepsilon=0 \tag{11}$$

Assuming the turbulence at the conditions of neutral equilibrium (the rate of turbulence production P_k equals the rate of dissipation $\rho\varepsilon$). Substituting Eq. (4) into Eq. (10) and Eq. (11), and combining both expressions P_k with Eq. (4), yields:

$$C_\mu=\left(\frac{-\overline{u'w'}(z)}{k(z)}\right)^2 \tag{12}$$

$$\varepsilon=C_\mu^{1/2}k(z)\frac{\partial u}{\partial z} \tag{13}$$

Given the hypothesis of constant shear stress, (Parente et al., 2011) assumed a height-dependent form of the C_μ parameter, which can be written as :

$$C_\mu(z)=\frac{u_*^4}{k(z)^2} \tag{14}$$

Thus, from Eq. (12), the turbulent kinetic energy can be written as:

$$k(z)=\frac{-\overline{u'w'}}{\sqrt{C_\mu}} \tag{15}$$

Nevertheless, after extensive wind tunnel experiments, the researchers (Juretic & Kozmar, 2013) noted that the rate between the dominant shear stress in ABL $-\overline{u'w'}$ and the turbulent kinetic energy $k(z)$ remained virtually invariant along the height, suggesting that the value C_μ is constant. Thus, in the case of neutral ABL, the closure constants of the $k-\varepsilon$ turbulence model should be adjusted. According to this condition, these constants can be established following the values provided below in Table 2:

Table 2 Values of the closure constants for the $k-\varepsilon$ model in the case of neutral ABL. (Sørensen et al., 2007)

Closure constant	C_μ	$C_{\varepsilon 1}$	$C_{\varepsilon 2}$	σ_k	σ_ε	κ
Neutral case	0.03	1.21	1.92	1.0	1.3	0.40

2.3 Inlet Boundary Conditions and Turbulence Model

2.3.1 Richard and Hoxey (RH) profile: constant shear stress $-\overline{u'w'}(z)=u_*^2$

According to (Yan et al., 2015), the shear stress in the turbulent flow may be regarded as constant and identical to wall shear stress in the inner surface of ABL. The inlet profiles for the fully developed flow in the horizontally homogeneous ABL can be expressed as follows, as suggested by (Richards & Hoxey, 1993):

$$U=\frac{u_*}{\kappa}\ln\left(\frac{z+z_0}{z_0}\right) \tag{16}$$

$$k=\frac{u_*^2}{\sqrt{C_\mu}} \tag{17}$$

$$\varepsilon=\frac{u_*^3}{\kappa(z+z_0)} \tag{18}$$

where u_* defines the friction velocity, and can be specified from the experimental data used in this work. z_0 is an aerodynamics roughness height and κ is the von Karman constant.

Therefore, by combining Eq. (16), Eq. (17), Eq. (18), and Eq. (11), the residual ε is given by the following formulation:

$$R_\varepsilon=\frac{(u_*)^4}{(z+z_0)^2}\left[\frac{(C_{\varepsilon 2}-C_{\varepsilon 1})\sqrt{C_\mu}}{\kappa^2}-\frac{1}{\sigma_\varepsilon}\right] \tag{19}$$

In accordance with (Pontiggia et al., 2009), if the Schmidt number σ_ε is equal to $\frac{\kappa_v^2}{(C_{\varepsilon 2}-C_{\varepsilon 1})\sqrt{C_\mu}}$, then R_ε would vanish, and the residual R_ε should be added as a source term in the transport equation of turbulent dissipation energy ε in order to achieve the mathematical coherence of the RH profile.

2.3.2 ESDU Shear Stress Profile: $-\overline{u'w'}(z)=u_*^2\left(1-\frac{z}{D_2}\right)^2$

The Engineering Science Data Unit (ESDU) profile is provided under experimental evidence (ESDU, 1985; Yang et al., 2009) and is used in computational wind engineering. This model can be employed to reduce the errors found in the RH profile, which is based on the hypothesis of constant shear stress along the ABL height. In contrast, the results from the experience show that the shear stress is variant throughout height and decreases vertically in the ABL flow around a flat plate. Hence, the turbulence profiles can be expressed as follows:

$$k(z)=\frac{u_*^2}{\sqrt{C_\mu}}\left(1-\frac{z}{D_2}\right)^2 \tag{20}$$

$$\varepsilon(z)=\frac{u_*^3}{\kappa(z+z_0)}\left(1-\frac{z}{D_2}\right)^2 \tag{21}$$

By substituting Eq. (20) and Eq. (21) in the transport Eq. (10) and Eq. (11) the residuals R_k (Eq.(22)) and R_ε (Eq. (23)), respectively, of k and ε are obtained:

$$R_k=\frac{2u_*^3\kappa}{\sqrt{C_\mu}D_2\sigma_k}\left(\frac{z}{D_2}-D_1\right)^2\left(\frac{4z}{D_2}-D_1\right) \tag{22}$$

$$R_\varepsilon=\frac{(u_*)^4}{(z+z_0)^2}\left[\frac{(C_{\varepsilon 2}-C_{\varepsilon 1})\sqrt{C_\mu}}{\kappa^2}-\frac{1}{\sigma_\varepsilon}\right] \tag{23}$$

However, to ensure the equilibrium of ABL, the residuals R_k and R_ε should be added to the transport equations of k and ε as source terms.

2.4 Near Wall Treatment

2.4.1 Standard Rough Wall Function

In the case of turbulent airflow in the ABL over a complex terrain, the Reynolds number is typically high. All the impacts of roughness on the wall surface on the airflow should therefore be taken into account in order to obtain accurate simulation results. Thus, the use of the wall function with rough modification is necessary in order for the $k-\varepsilon$ turbulence model to decrease the high number of mesh cells necessary close to the wall.

In this work, however, the CFD simulations are performed with the commercial code COMSOL Multiphysics, which is based on the Finite Element Method (FEM) (COMSOL, 2016). Hence, the fully rough k_s - type wall for average velocity in the COMSOL code is given by the following expression:

$$\frac{\left|U_{\delta_w}\right|}{u_\tau}=\frac{1}{\kappa}\ln\left(E\delta_w^+\right)-\Delta B\left(k_s^+\right) \tag{24}$$

where u_τ is the friction velocity, E is an integration constant $(E=9.3)$, and δ_w^+ is the dimensionless distance from the wall defined as $\delta_w^+=\rho u_\tau\frac{\delta_w}{\mu}$, with $u_\tau=C_\mu^{1/4}\sqrt{k}$. The function $\Delta B\left(k_S^+\right)$ depends on the dimensionless equivalent roughness height $k_s^+=k_s u^*/\nu$ where k_s defines the sand-equivalent roughness height of the local terrain.

This can be used in different forms, according to the equivalent sand grain roughness height. In particular, $k_S\geq 90$, Eq. (24) can be expressed in terms of the equation below:

$$\begin{aligned}\frac{\left|U_{\delta_w}\right|}{u_\tau}&=\frac{1}{\kappa}\ln\left(E\delta_w^+\right)-\frac{1}{\kappa}\ln\left(1+C_s k_s^+\right)\\&=\frac{1}{\kappa}\left(\frac{E\delta_w^+}{1+C_s k_s^+}\right)\approx\frac{1}{\kappa}\ln\left(\frac{E\delta_w^+}{C_s k_s^+}\right)\end{aligned} \tag{25}$$

where C_s is the roughness constant with the value of 0.26 in COMSOL software. The purpose of this constant is to take the nature of roughness into consideration.

In the study by (Blocken et al., 2007), the authors briefly set out the four basic requirements that must be addressed to achieve adequate ABL numerical simulation. To fulfill all of these requirements, (Yan et al., 2015), it is proposed that the setting parameter C_s should be a variable rather than a constant, such that as provided by commercial codes.

$$C_s=\frac{Ez_0}{K_s} \tag{26}$$

In consequence, this can lead to large computational cells and to an erroneous resolution, since one of the requirements is that the distance from the wall between the first computational point of the wall-adjacent cell δ (see Fig. 2) should be larger than the equivalent roughness height k_s, i.e. $(\delta_w \succ k_s)$(Franke et al., 2004; Yan et al., 2015).

2.4.2 Modified Rough Wall Function

In accordance with the conditions mentioned in the

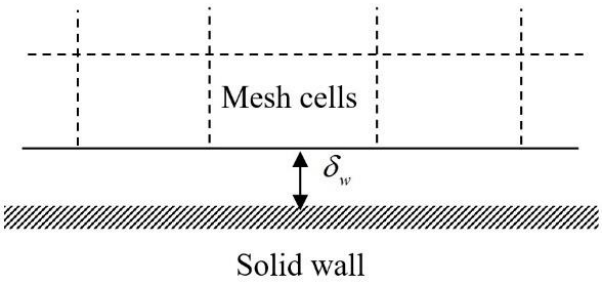

Fig. 2. Distance from the wall to the computational domain.

previous section, and using the maximum value, $k_s=\delta_w$, C_s can be calculated from Eq. (27) below for each cell using the aerodynamic roughness length z_0, and is a suitable option for obviating the requirement $(\delta_w \succ k_s)$. Its conditions are available for a fully rough regime.

$$C_s=\frac{Ez_0}{k_s}\approx\frac{Ez_0}{\delta_w} \tag{27}$$

In the research conducted by (Yan et al., 2015), it was indicated that if $z_p=3.695z_0$, then sufficient production of kinetic energy could be obtained. Thus, k_s is defined as $k_s=\delta_w=3.695z_0$ and depends on the parameter δ_w that is used in COMSOL. Hence, the value C_s can be found by using Eq. (27). The implementation of this equation can be performed by using the User Defined Equation (UDE) in COMSOL Multiphysics.

The boundary conditions applied on the wall to specify the velocity and turbulent dissipation are taken from (Richards & Hoxey, 1993; Parente et al., 2010), and consist of using an equation $u_\tau=C_\mu^{1/4}\sqrt{k}$ with the definition of friction velocity on the wall. However, this differs regarding the use of the parameter defining the distance from the wall δ_w on COMSOL, as follows:

$$\left|U_{\delta_w}\right|=\frac{u_\tau}{\kappa}\ln\left(E^{'}\delta_w^+\right) \tag{28}$$

where $E^{'}=\frac{\nu}{z_0 u_\tau}$;

$$\varepsilon_w=\frac{C_\mu^{3/4}k^{3/2}}{\kappa\delta_w^+} \tag{29}$$

Since the COMSOL software uses the scalable wall function Eq. (30) above for the near wall treatment (COMSOL, 2016), some differences exist in the

literature referred to in the foregoing. The scalable wall function is used to simplify the use of the software, as well as to avoid the consequences that may arise from the refinement of the mesh. This function depends on the fixed value of the distance from the wall $\delta_w^+ = 11.06$, the dimensionless equivalent roughness height k_s^+, and the dimensionless height of the first mesh cell h^+, respectively. We note that, for the limit of the dimensionless distance to the wall, it can in most cases take the maximum condition, which indicates the value of $\frac{k_s^+}{2}$, implying that δ_w^+ is always less than k_s^+. This condition leads to ambiguities in the requirements mentioned in the literature.

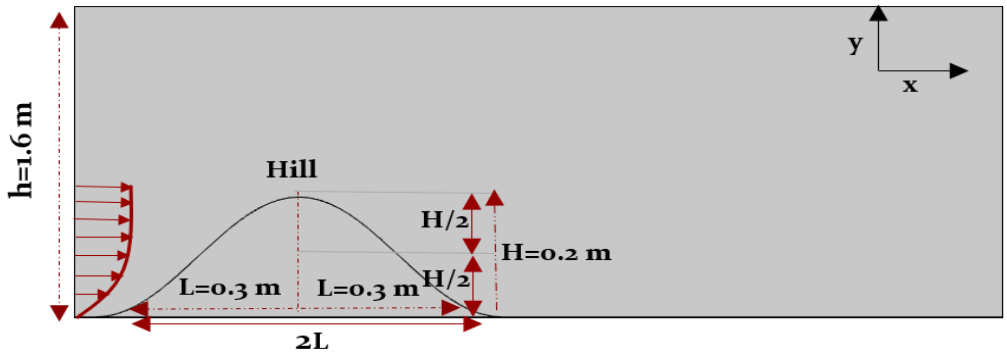

Fig. 3. Configuration of the computational domain with presence of the hill model (characteristic measures of the CRIACIV BLWT data).

$$\delta_w^+ = \max\left(11.06, \frac{h^+}{2}, \frac{k_s^+}{2}\right) \tag{30}$$

As mentioned before, δ_w is programmed as a fixed parameter. Moreover, it would be advisable to implement a new expression to ensure a variable distribution δ_w^+ as a function of the aerodynamic roughness z_0 in order to remedy the limitation of the standard wall function with roughness. Hence, the idea that all the parameters must be varied according to z_0. To that end, we have had recourse to a variant of the dimensionless height of the first mesh cell h^+, in such a way that it takes into account the aerodynamic roughness z_0 (Eq. (31)):

$$h^+ = \frac{\left(C_\mu^{1/4} k^{1/2}\right)\left(h + z_0\right)}{\nu} \tag{31}$$

This approach can ensure two conditions at the same time. First of all, it ensures the compatibility of the inflow condition and the wall function by taking into account all the effects of roughness. Secondly, it facilitates the convergence of the calculation and reduces the need for a refinement of the mesh in order to control the points close to the wall, which cannot be strictly controlled.

3. NUMERICAL CASES AND EXPERIMENTAL SETUP

The first measure regarding the validation of the suggested approach is to demonstrate that its results consist of fully developed inlet velocity and turbulence profiles, and that they are maintained along a flat terrain (empty domain). After that, the simulation of turbulent flow over a hill is presented, with aim of studying the performance of the model in complex and rough terrain.

3.1 Details of the CRIACIV Boundary Layer Wind Tunnel

Distribution of the turbulent airflow over a hill model (CRIACIV Boundary Layer Wind Tunnel BLWT) (Augusti et al., 1995) was measured from the wind tunnel to the ABL at a 1:300 scale for applying the wind turbines and a hilly terrain model to identify the significante prototype values. This experiment highlighted the hill model located upstream of a wind farm. The neutrally stratified conditions of ABL simulation windward of the hill model are conducted by means of the (Counihan, 1969) with the basic principles of this procedure described in (Kozmar, 2011; Kozmar et al., 2016, 2018). In this wind tunnel experience, the flow velocity in the test section can be adjusted from 0 m/s to 30 m/s to perform an ABL with strong wind under neutral conditions.

The shape of the hill is considered with a profile given by the cos expression (Eq. (32)):

$$\begin{aligned} y_h(x) &= H\cos^2\left(\pi x/2L\right) \\ y_h(x) &= 0 \end{aligned} \tag{32}$$

where H represents the hill height, L defines the half-distance between the upwind and downwind of the hill (see Fig. 3).

3.2 Setting of Inlet Profiles

The mean input velocity condition in the main wind direction (x) was fixed on the basis of Eq.(16), with friction velocity $u_* = 1.2m/s$ and length of aerodynamic roughness $z_0 = 0.006m$. This profile matches a reference of mean velocity at the hill-model height $U_{ref} = 10m/s$. The Reynolds number was fixed as $R_e \approx 1.3 \cdot 10^5$. Inlet profiles of turbulence parameters (y) and $\varepsilon(y)$ are calculated by Eq.(17) and Eq. (18) for case 1 (RH profiles), and by Eq.(20) and Eq. (21) for case 2 (ESDU profiles).

3.3 Setting of Computational Domain and Mesh Configuration

The computational domain of the first study was presented as a 2D empty rectangle (without a hill) with

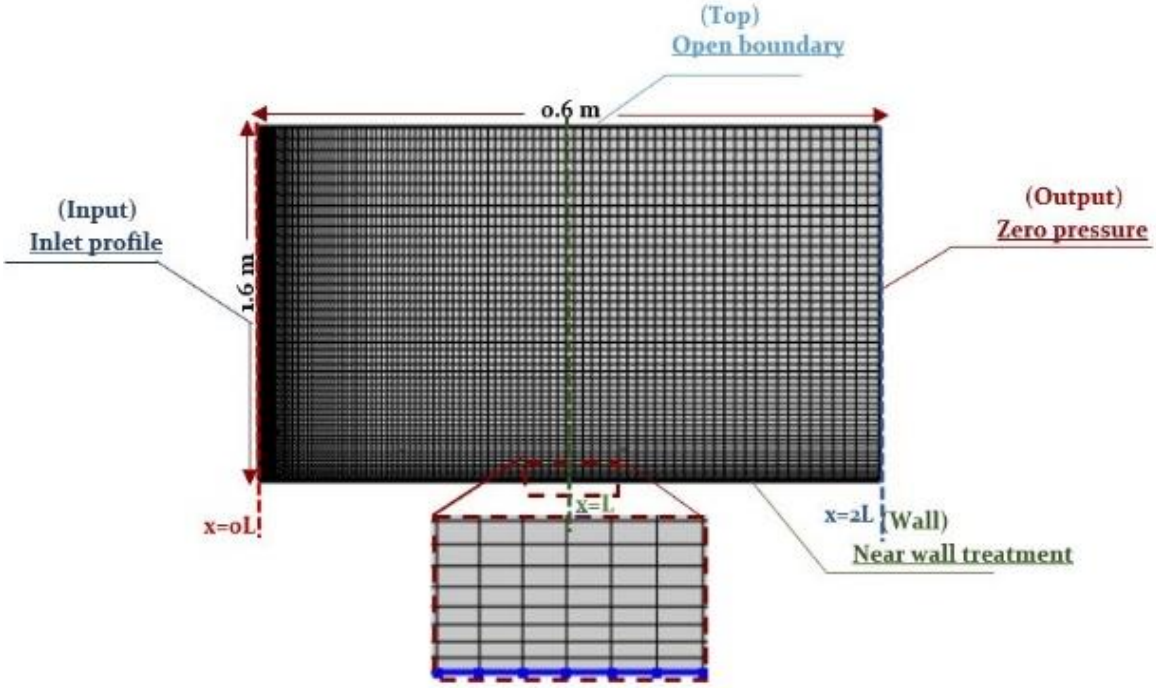

Fig. 4. Mesh configuration and boundary conditions set for the computational domain (Flat Terrain).

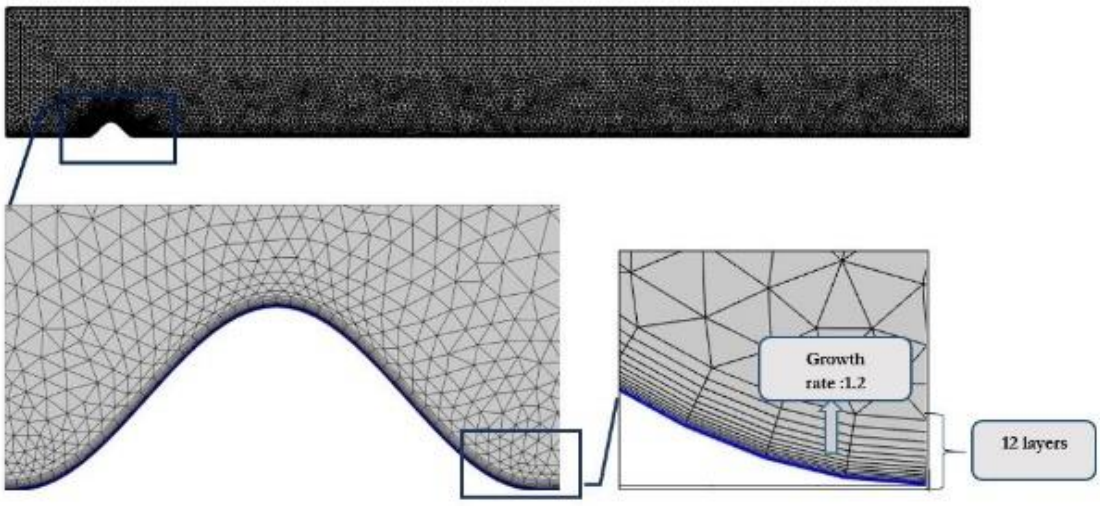

Fig. 5. Representation of a hybrid mesh over a topographic model. Zoom mesh view of the hill surface.

1.6m of height and 0.6m of length. This domain contains the fluid flow distribution, meshed and converted into a two-dimensional grid. The quadratic elements of the structured mesh are presented as distributions throughout the domain; in particular, in the vertical (y) and horizontal (x) directions. In addition, the refinement was carried out in the vicinity of the inlet and close to the wall surface (Fig. 4) in order to capture any significant change in the variables more precisely. On the other hand, the total number of mesh elements is 5000 quadratic elements with a minimum mesh quality of 1.

The second case is for the CFD modeling of airflow over a hill model. In this study, the domain size is shown in Fig. 3 to simulate the hill inside the neutral ABL. The simulation domain length extends upstream from the hill for a distance of $-6.5H$ m and downstream for a distance of $53.5H$ m, with a hill length of $2L = 0.6m$ asymmetry and a domain height of $1.6m$, such that the height of the hill is $H = 0.2m$. In the present study, a hybrid mesh, which is used in COMSOL Multiphysics (see Fig. 5), corresponds for the present simulation to a structured mesh near the isolated hill, and contains 12 layers with a thickness of the first cell of the boundary layer equal to $\delta = 3.695 z_0$. On the other hand, an unstructured mesh is used for the other part of the domain, with a maximum triangular cell size of 72.10^{-3} and a minimum size of 32.10^{-4}. Several types of grid mesh were tested in this

study, finer mesh results providing a more accurate solution. The hybrid mesh contains *16202* elements in the whole domain, which corresponds to *3684* quadratics for the boundary layer grid and *12518* triangles for the other part of the domain. As shown in Fig. 5, the refinement was chosen to correspond to the level of flow mesh refinement that approximates an object in the fluid domain.

Table 3 Summary of the boundary conditions used for flat terrain

	Standard approach	Modified approach
Inlet	RH profile: Eq. (16), Eq. (17), Eq. (18) ESDU profile: Eq. (16), Eq. (20), Eq. (21)	RH profile: Eq. (16), Eq. (17), Eq. (18) ESDU profile: Eq. (16), Eq. (20), Eq. (21)
Outlet	$P = P_{atm}$	$P = P_{atm}$
Open	$\frac{\partial}{\partial n}(u, v, k, \varepsilon) = 0$	$\frac{\partial}{\partial n}(u, v, k, \varepsilon) = 0$
Wall	Standard wall function with roughness modification, Eq. (26) and Eq. (30) defined by COMSOL software.	Development of wall function, based on aerodynamic length (Eq. (27), Eq. (28), Eq. (29), and Eq. (31)).

Table 4 Summary of the different entry profile conditions and the corresponding modifications to the $k-\varepsilon$ turbulence model

	C_μ	σ_ε	S_k	S_ε
RH profile	$\frac{u_*^4}{k(z)^2}$	$\frac{\kappa_v^2}{(C_{\varepsilon 2} - C_{\varepsilon 1})\sqrt{C_\mu}}$	$\frac{\sqrt{C_\mu}\kappa_v}{u_* \sigma_k} \frac{\partial}{\partial z}\left[(z + z_0) k(z) \frac{\partial k(z)}{\partial z}\right]$	$\frac{(u_*)^4}{(z + z_0)^2}\left[\frac{(C_{\varepsilon 2} - C_{\varepsilon 1})\sqrt{C_\mu}}{\kappa_v^2} - \frac{1}{\sigma_\varepsilon}\right]$
ESDU profile	$\frac{u_*^4}{k(z)^2}$	$\frac{\kappa_v^2}{(C_{\varepsilon 2} - C_{\varepsilon 1})\sqrt{C_\mu}}$	$\frac{2u_*^3 \kappa_v}{\sqrt{C_\mu} D_2 \sigma_k}\left(\frac{z}{D_2} - D_1\right)^2\left(\frac{4z}{D_2} - D_1\right)$	$\frac{(u_*)^4}{(z + z_0)^2}\left[\frac{(C_{\varepsilon 2} - C_{\varepsilon 1})\sqrt{C_\mu}}{\kappa_v^2} - \frac{1}{\sigma_\varepsilon}\right]$

3.4 Solver Setup

For both study cases, CFD simulations were conducted by using the COMSOL Multiphysics steady-state 2D. Simulations were performed with a Reynolds number $R_e \approx 1.3 \cdot 10^5$ at the top of the hill. The turbulence quantities were solved separately from momentum and pressure using a segregated solver. Discretization will be performed by using a $P_2 - P_1$ scheme to solve the velocity-pressure coupling. While the linear scheme is adopted for pressure, the quadratic schemes (second-order element) are adopted for momentum and turbulence quantities. Once the consecutive results of the CFD numerical simulation cease to vary dramatically by the addition of more iterations, the solution converges. All the simulations reported in this work have converged to a solution with a relative error of less than 10^{-5}.

4. CFD SIMULATION OF HORIZONTAL HOMOGENEITY ABL FLOW OVER FLAT TERRAIN

4.1 Boundary Conditions

The details of the physical parameters of the boundary conditions presented in Fig. 4 are given below in Table 3. The domain, velocity and turbulence quantities are fixed at the inlet of the boundary domain by using two tests of the conditions; the RH profile and ESDU profile, respectively. The ABL properties, which will be employed in these conditions, are established with values cited in Section 3.2. Furthermore, a relative pressure $0Pa$ is applied in the outlet boundary condition for a smooth output of the flow outside of the domain. Hence, the top boundary is modeled as a slip-open boundary with constant shear stress U for a homogeneous ABL. It should be noted that two approaches to processing the results are used for the wall boundary conditions. Firstly, the standard approach for the first test of the work, based on a standard rough wall function implemented in COMSOL Multiphysics to describe the inhomogeneity within flat terrain, and secondly, a test based on the description of the horizontal homogeneity of the ABL, which will be used in the development of the wall function mentioned in Section 2.4.2 with the addition of the source terms to the transport equations, as presented in Section 2.3.

4.2 Impact of the Modeling Approach on the Horizontal Homogeneity ABL: Results and Discussions

Equilibrium ABL is performed in the flat terrain as an empty domain with a comparison of the inlet, middle, and outlet profiles in the positions *x=0L*, *x= L*, and *x=2L* as shown in Fig. 4. Note that *L* defines half the length of the domain.

Figure 6 and Fig.7 provide comparison profiles of the mean streamwise wind speed u, turbulence kinetic energy k, and turbulence dissipation rate ε for the three positions indicated in Fig.4. However, Fig. 6 is for the CFD simulations assessed with a standard approach, while Fig. 7 is for modified approach results.

As may be observed in Fig. 6, for the mean wind speed, a good consistency is shown, with a shift close to the wall between inlet, middle, and outlet profiles for two sets of inlet RH and ESDU conditions. Therefore, the turbulence kinetic energy k given at the inflow section is well conserved on the top region of the domain.

However, a slightly marked difference near the ground can be seen when applying RH and ESDU profiles. Moreover, the turbulence dissipation energy ε in the down region of the boundary layer shows a strong degradation in both of the cases tested, while in the upper part, three positions are approximately preserved all along the domain (from a height of *0.3m*). As discussed in the sections above, it can be concluded that the discrepancies between the predicted inlet, middle, and outlet profiles can further be observed in the down region of the ABL. Globally, both cases of the study prove that two inlet conditions tested alone are not enough to

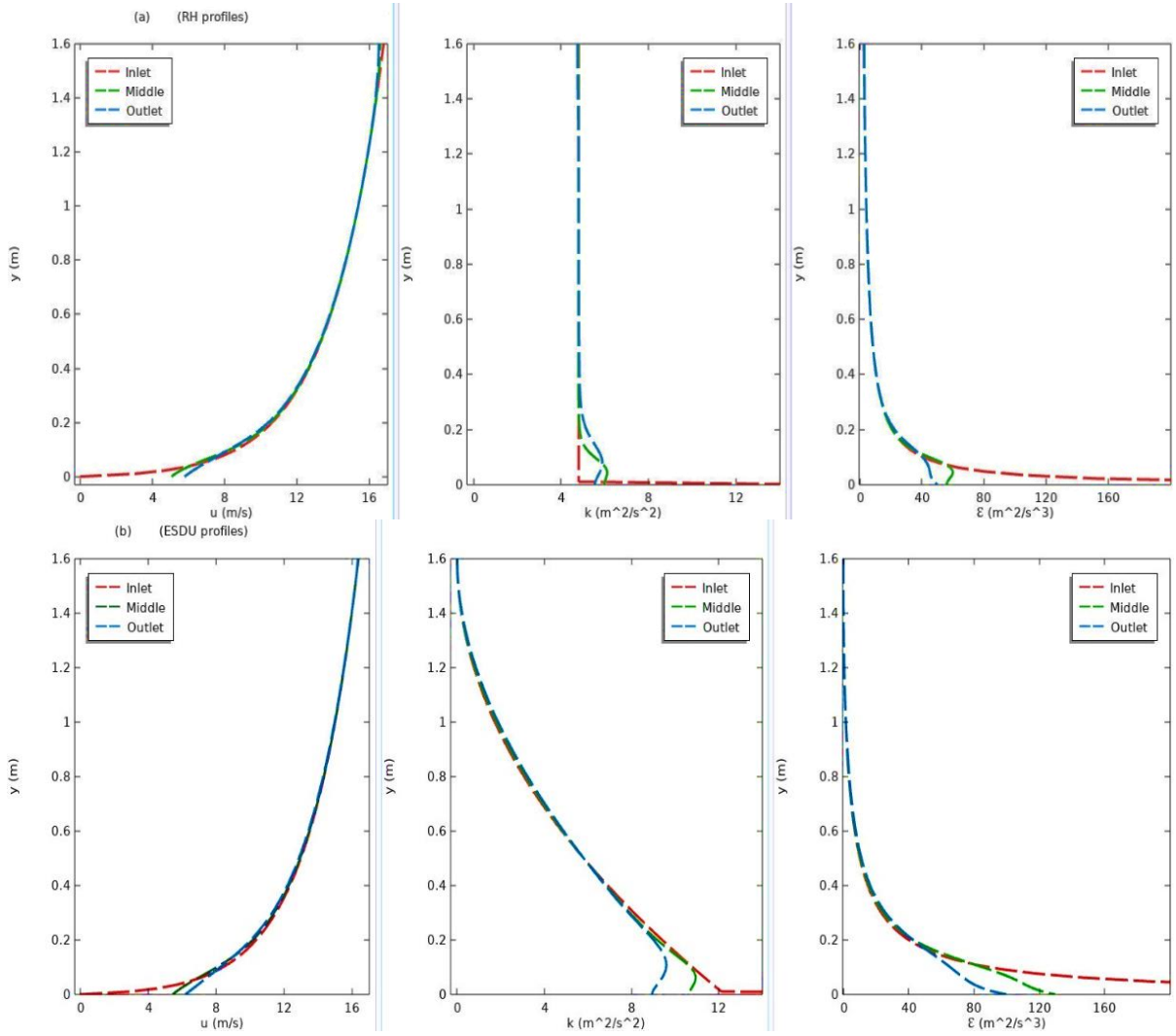

Fig. 6. Representation of vertical profiles of u, k and ε at x=0L, x=L, x=2L for the RH profile (a) and the ESDU profile (b), obtained by using a standard approach.

generate an equilibrium ABL through the use of $k-\varepsilon$ the turbulence model and the standard rough wall function. This confirms the incompatibility of the inlet and ground conditions used.

Figure 7 discusses the behavior of the remedial turbulence model $k-\varepsilon$, coupled with the development of rough wall function in order to simulate a horizontally homogeneous ABL flow under two different sets of inlet conditions. The turbulence profiles of k and ε, with their respective changes to the closure model, are briefly summarized below in Table 4. The S_k, S_ε, and modified σ_ε are implemented in COMSOL software through the use of UDE. The other conditions are also presented in Table 4. Similarly, the closure constants $k-\varepsilon$ are modified according to Table 2 for the neutral ABL simulations.

Figure 7 shows that, in general, in the case of the RH profile, both profiles of velocity u and turbulence quantities k and ε are well conserved throughout the x-direction of the whole domain. Moreover, the results obtained within the framework of the ESDU profile show good consistent results of the ABL flow profiles for velocity u and turbulence dissipation energy ε. Therefore, the turbulence kinetic energy k profile shows satisfactory results when compared with the standard approach results. Nevertheless, the profile of ESDU still behaves better than the condition of RH with respect to the adaptation of the variant throughout height, and decreases vertically in the ABL flow around a flat plate.

It is possible that a considerable homogeneity of the neutral ABL flow simulation could be obtained under uniform expression of the inflow condition and the

associated modifications to the $k-\varepsilon$ model. Furthermore, the development rough wall function approach and the use of source terms, S_k, S_ε and σ_ε in transport equations also play a significant role in maintaining the velocity and turbulence homogeneity throughout the whole domain.

5. NUMERICAL SIMULATION OF TURBULENT WIND FLOW OVER A 2D HILL: RESULTS AND DISCUSSIONS

After successfully simulating a horizontal homogeneous boundary layer and quantitatively evaluating the impacts of different profiles on flow

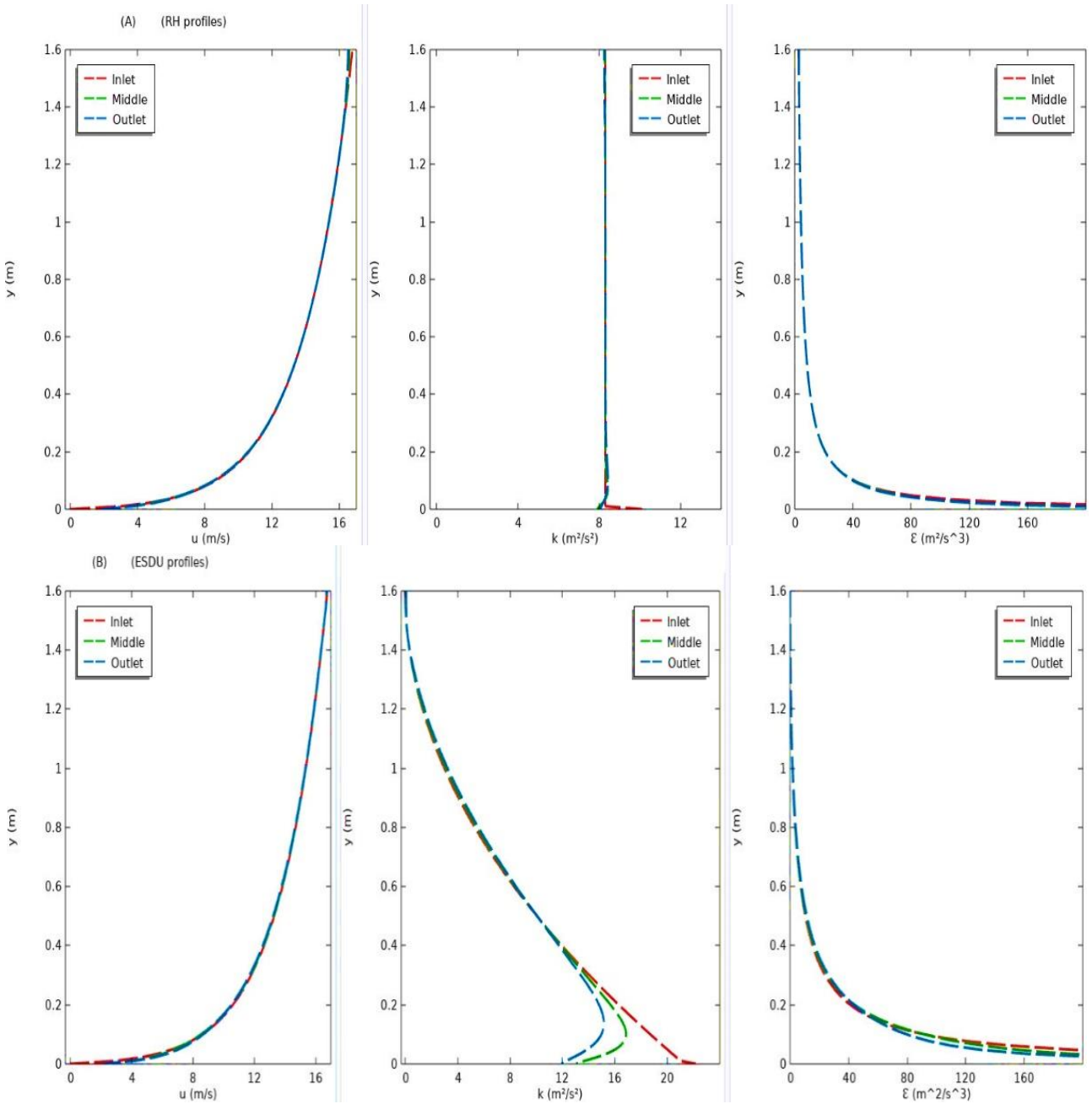

Fig. 7. Representation of vertical profiles of u, k and ε at x=0L, x=L, x=2L The RH profile (A) and the ESDU profile (B), obtained by using a modified approach with the addition of the source term.

development in flat terrain, as well as validations of the model configuration and calculation method, these methods will now be employed in the numerical study of the effect of the topography of a hill model, with the main aim of verifying the influences of the different atmospheric boundary conditions on the development of the turbulent wind flow around a hill.

Firstly, a comparison of the topographic effects on the surface wind speed is made between observations from wind tunnel measurements and CFD numerical simulation results.

The evolution of streamwise wind speed profiles u (see Fig. 8), turbulent kinetic energy k (see Fig. 9), and turbulent intensity I (see Fig.10) are also compared with

wind tunnel data results, in order to study separately the effects of the inlet conditions RH and ESDU $k-\varepsilon$ turbulence model and modified rough wall function used in this work, in three positions over hill, upstream *x/H=-1.5*, top hill *x/H=0* and downstream hill *x/H=1.5*. The agreement between the wind tunnel data and CFD results is good, although some deviations from the coherent are observed in near-ground regions. This is due to the measurement taken in an offset height of the wall during the experiment, also in the recirculation region in this return to the prediction of each condition used at the inlet.

In the present study, we investigate the elements of turbulence flow such as intensity and turbulent kinetic energy k in order to understand the structure of turbulent flow over the hill. The vertical profiles of turbulence intensity I presented in Fig.9 for different positions around the hill show that on the upstream of the hill *x/H=*

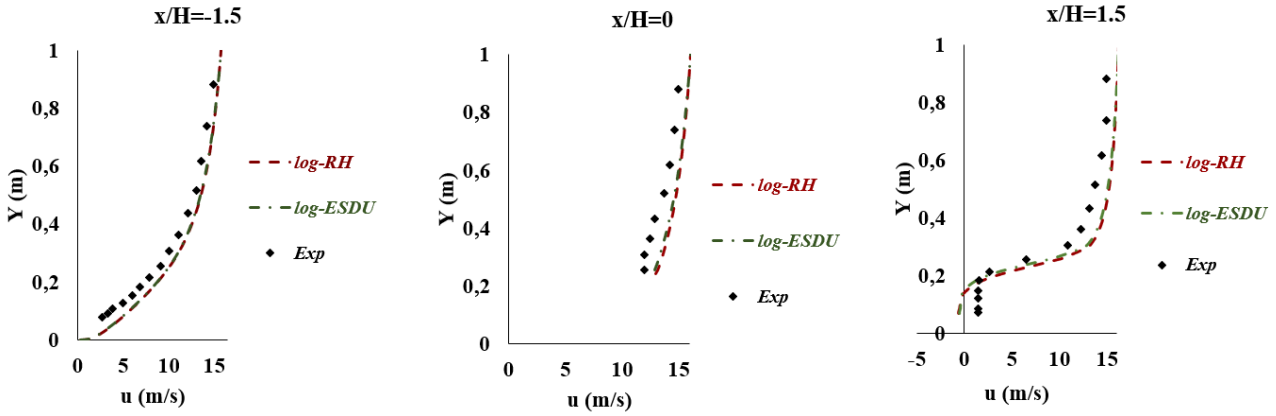

Fig. 8. Streamwise wind speed profiles for the different inlet conditions RH and ESDU for the $k-\varepsilon$ turbulence model in comparison with the wind tunnel experience in the three positions (x/H=-1.5; x/H =0; x/H= 1.5).

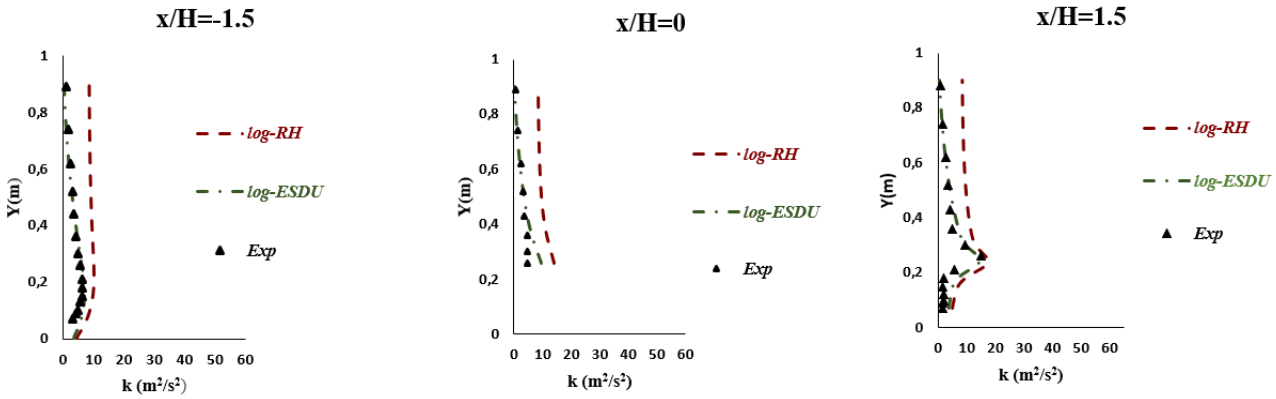

Fig. 9. Turbulence kinetic energy k profiles for the different inlet conditions log-RH and log-ESDU for the $k-\varepsilon$ turbulence model in comparison with the wind tunnel experience in the three positions (x/H=-1.5; x/H =0; x/H= 1.5).

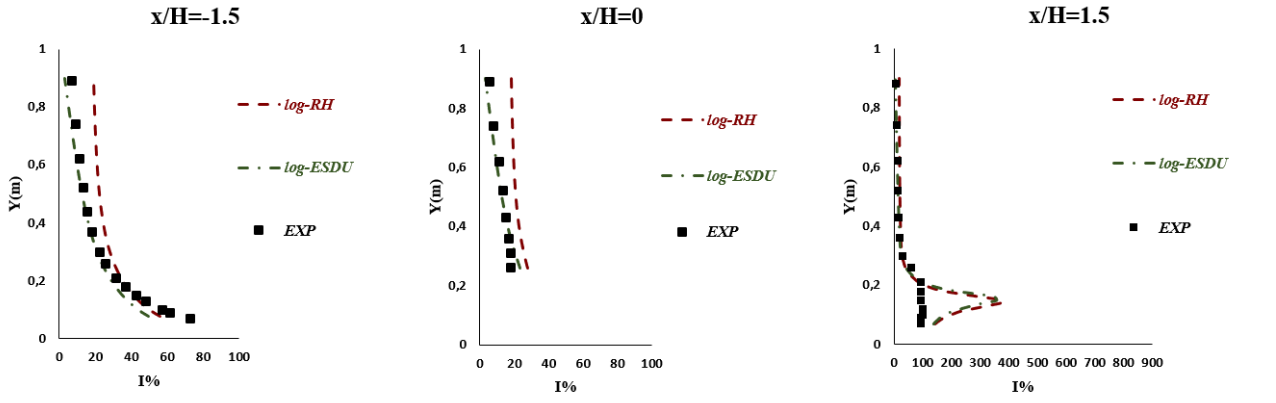

Fig. 10. Turbulence intensity I profiles for the different inlet conditions RH and ESDU for the $k-\varepsilon$ turbulence model in comparison with the wind tunnel experience in the three positions (x/H=-1.5; x/H =0; x/H= 1.5).

Journal of Applied Fluid Mechanics, Vol. 16, No. 8, pp. 1515-1530, 2023.
Available online at www.jafmonline.net, ISSN 1735-3572, EISSN 1735-3645.
https://doi.org/10.47176/jafm.16.08.1702

-1.5, the important intensity I values are expected near the wall and start to decrease according to the height, i.e. when the wind speed increases.

However, very low values of the turbulence intensity are recorded far from the top of the hill *x/H=0* (see Fig.9 at the center). This is due to the acceleration of the speed at this location. Due to the influence of an adverse pressure gradient, at the downstream side of the hill *x/H=1.5* (see Fig.9, right) the turbulence intensity increases gradually along the downstream side of the hill and presents peaks that are about half the hill height, and more precisely in the vortex zone, when the wind speed decreases in the same region. This implies that the presence of roughness generates more turbulence.

Moreover, it is noted that the predictions obtained based on the RH profile are slightly higher than those of the ESDU profile at the top, in the recirculation region, and in the wake region of the hill, while the results are identical in the upper edge. This behavior is due to the condition that turbulence profiles with the ESDU profile should take into account a decrease in turbulence

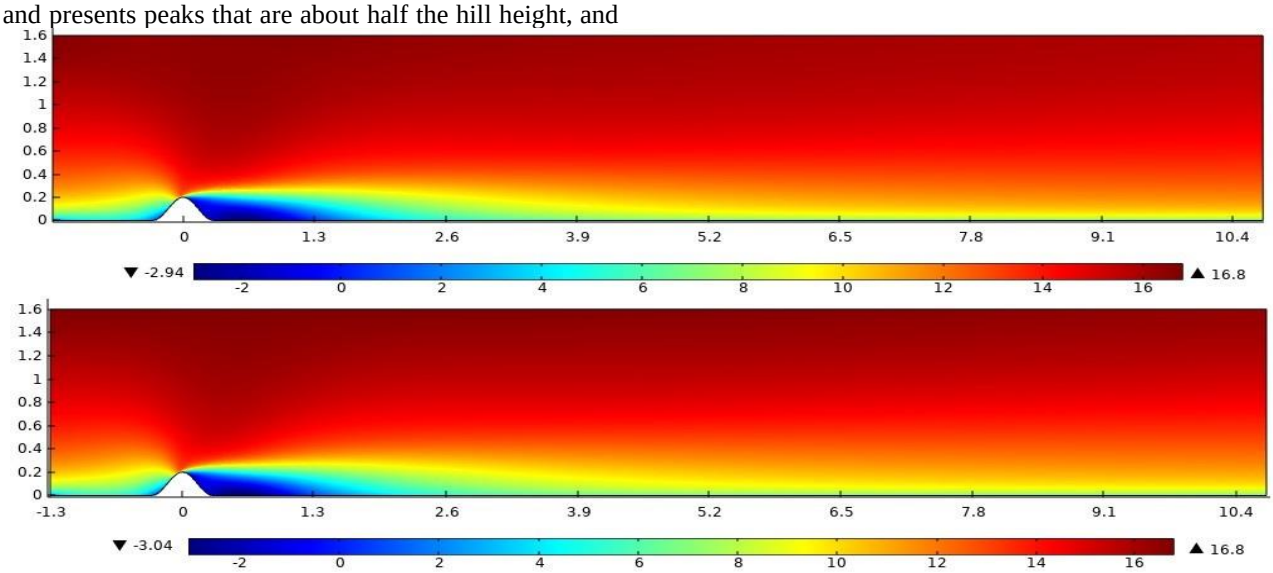

Fig. 11. Contours of the streamwise wind speed component around the hill with the two inlet conditions used (line 1: RH profile; line 2: ESDU profile).

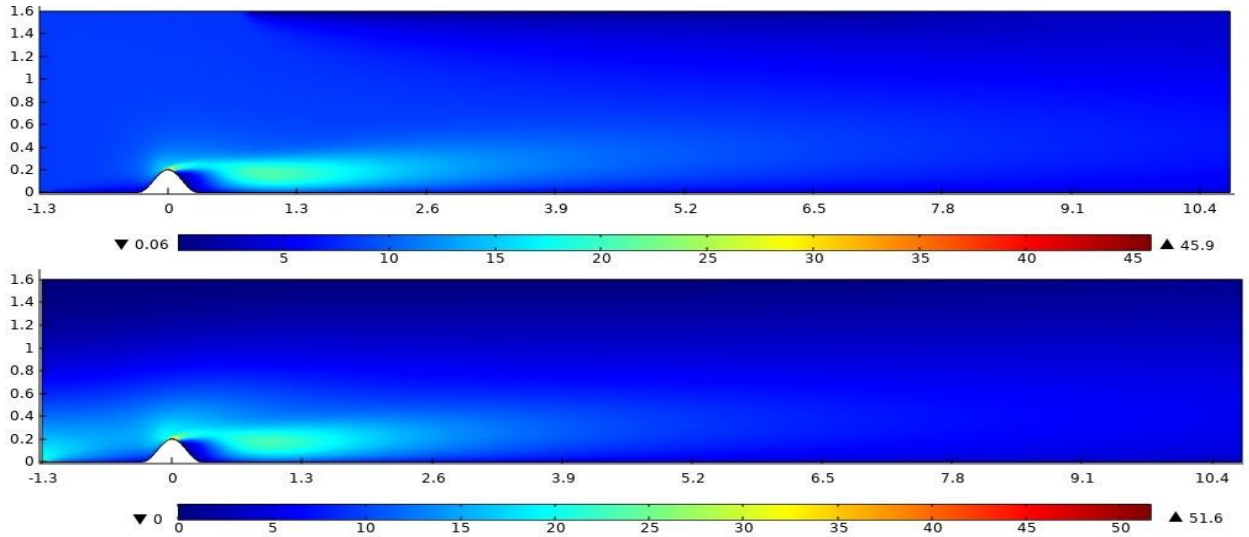

Fig. 12. Contours of the turbulent kinetic energy around the hill with the two inlet conditions used (line 1: RH profile; line 2: ESDU profile).

parameters with altitude instead of the constant condition used by the RH profile.

Figure 11 and Fig.12 present the contours of the predicted velocity and turbulent kinetic energy in the considered terrain. The streamwise wind speed (see Fig.

11) is briefly presented somewhat upstream, at the top and downstream of the hill. The position of the vortex center, which is downstream of the downslope of the hill depends on the behavior of the upstream flow. The rough surface reduces the upward velocity near the wall, leading to an increase in turbulence and consequently a decrease in kinetic energy (see Fig.12). The attenuation of turbulence kinetic energy is reflected by the further distance of the vortex center from the downward slope downhill.

The presence of complex topography in the terrain is responsible for the separation of the approach boundary layer near the wall surface (see Fig.11). According to the construction of this phenomenon, the boundary layer is disturbed and a thin shear layer is formed. The shear layer folds down and attaches to the surface. It is likely to be subject to the negative pressure gradient effects that are responsible for the first half of the shear layer, which is not influenced by the presence of the wall and thus behaves as a free shear layer. Moreover, towards the ground and more precisely towards the reattachment zone in the other part of the shear layer, the turbulence levels are more intense in the separated shear layer compared to the other regions of the flow, as can be observed in Fig. 10, and this is due to strong interaction between the shear layer and the wall.

The level of turbulent kinetic energy increases as the flow develops from the point of separation and attends a maximum at the top of the shear layer. The important value of the turbulent kinetic energy is positioned at the level of the hill height, as shown in Fig. 9 (on the right, *x/H=1.5*). On the other hand, the turbulent kinetic energy gradually disappears after the reattachment region and the flow starts to regenerate.

Regarding, the turbulent kinetic energy for both cases of RH and ESDU profiles (Fig. 12), the results yield an adequate description of the wake part behind the hill, which shows that the turbulence model modified conditions used in the current work is able to model turbulence parameters decreasing with altitude, and achieves a satisfactory accuracy. On the other hand, the blocking caused on the windward side of the hill reduces the kinetic energy of the up flow and influences the dynamics of the boundary layer in the obstacle wake.

6. Conclusion

In this study, a developed approach based on z_0-type scalable wall function has been proposed to allow for adequate predictions of CFD numerical simulation of horizontal homogeneous ABL profiles based on the k-ε turbulence model by using COMSOL Multiphysics. Firstly, the approach was verified in flat terrain (Empty domain) with two inlet conditions. The findings demonstrated that the horizontal homogeneity of simulated ABL flows was good. Secondly, the hill surface effects were examined with the combined use of the presented approach and two inflow profiles, such as, RH and ESDU. The results agreed with the CRIACIV BLWT experiment data. It shows that the conjunction of the proposed approach and both inlet boundary conditions can minimize the errors and provide fairly good correspondence.

On the other hand, the results have shown that the ESDU profile gives more accurate results and agree well with experimental data than the RH profile, in terms of turbulent kinetic energy and intensity turbulent.

The outcomes of the research are anticipated to be of common benefit and useful application for scientists and engineers advanced in wind energy.

The study findings can also improve the accuracy and reliability of CFD simulations, leading to better design and operation of various engineering structures, such as wind turbines and buildings, in hilly terrains. In addition, the presented approach can be easily adapted to an accurate estimation of wind speed, which has a major impact on choosing wind turbine positions in wind farms and on power production.

CONFLICT OF INTEREST

The authors declare that they have no known competing financial interests or personal relationships that could have appeared to influence the work reported in this paper.

AUTHOR CONTRIBUTION:

All authors contributed to the study conception and design. Material preparation, data collection and analysis were performed by [Amahjour Narjisse], [Sofi Anas], [Rodríguez Galván, José Rafae], [El Kharrim Abderrahman] and [Khamlichi Abdellatif]. The first draft of the manuscript was written by [Amahjour Narjisse] and all authors commented on previous versions of the manuscript. All authors read and approved the final manuscript.

REFERENCES

Abu-Zidan, Y., Mendis, P., & Gunawardena, T. (2020a). Impact of atmospheric boundary layer inhomogeneity in CFD simulations of tall buildings. *Heliyon*, *6*(7), e04274. https://doi.org/10.1016/j.heliyon.2020.e04274

Abu-Zidan, Y., Mendis, P., & Gunawardena, T. (2020b). Impact of atmospheric boundary layer inhomogeneity in CFD simulations of tall buildings. *Heliyon*, *6*(7). https://doi.org/10.1016/j.heliyon.2020.e04274

Augusti, G., Spinelli, P., Bartoli, G., Borri, C., Giachi, M., & Giordano, S. (1995). *The C.R.I.A.C.I.V. Atmospheric Boundary Layer Wind Tunnel*. Proceedings of the 9th International Conference on Wind Engineering (ICWE).

Blocken, B., Stathopoulos, T. & Carmeliet, J. (2007a). CFD simulation of the atmospheric boundary layer: wall function problems. *Atmospheric Environment*, *41*(2), 238–252. https://doi.org/10.1016/j.atmosenv.2006.08.019

Blocken, B., Carmeliet, J. & Stathopoulos, T. (2007b). CFD evaluation of wind speed conditions in passages between parallel buildings-effect of wall-

function roughness modifications for the atmospheric boundary layer flow. *Journal of Wind Engineering and Industrial Aerodynamics*, *95*(9–11), 941–962. https://doi.org/10.1016/j.jweia.2007.01.013

COMSOL. (2016). *Guide COMSOL: Introduction to COMSOL Multiphysics*.

Counihan, J. (1969). An improved method of simulating an atmospheric boundary layer in a wind tunnel. *Atmospheric Environment*, 3(2), 197–214. https://doi.org/10.1016/0004-6981(69)90008-0

ESDU. (1985). *Characteristics of atmospheric turbulence near the ground. Part II: single point data for strong winds (neutral atmosphere)*. Data Item 85020, Engineering.

Hargreaves, D. M., & Wright, N. G. (2007). On the use of the k –epsilon model in commercial CFD software to model the neutral atmospheric boundary layer. *Journal of Wind Engineering & Industrial Aerodynamics*, *95*, 355–369. https://doi.org/10.1016/j.jweia.2006.08.002

Franke, J., Hirsch, C., Jensen, A. G., Krüs, H. W., Schatzmann, M., Westbury, P. S., Miles, S. D., Wisse, J. A., & Wright, N. G. (2004). *Recommendations on the Use of CFD in Wind Enginnering.* Proceedings of the International Conference on Urban Wind Engineering and Building Aerodynamics, in: Van Beeck JPAJ (Ed.), COST Action C14, Impact of Wind and Storm on City Life Built Environment.

Juretic, F., & Kozmar, H. (2013). Computational modeling of the neutrally stratified atmospheric boundary layer flow using the standard k – e turbulence model. *International Journal of Wind Engineering and Industrial Aerodynamics*, *115*, 112–120. https://doi.org/10.1016/j.jweia.2013.01.011

Kozmar, H. (2011). Characteristics of natural wind simulations in the TUM boundary layer wind tunnel. *Theoretical and Applied Climatology*, *106*(1–2), 95–104. https://doi.org/10.1007/s00704-011-0417-9

Kozmar, H., Allori, D., Bartoli, G., & Borri, C. (2016). Complex terrain effects on wake characteristics of a parked wind turbine. *Engineering Structures*, *110*, 363–374. https://doi.org/10.1016/j.engstruct.2015.11.033

Kozmar, H., Allori, D., Bartoli, G., & Borri, C. (2018). Wind characteristics in wind farms situated on a hilly terrain. *Journal of Wind Engineering & Industrial Aerodynamics*, 174(January), 404–410. https://doi.org/10.1016/j.jweia.2018.01.008

Lubitz, W., & White, B. R. (2007). Wind-tunnel and field investigation of the effect of local wind direction on speed-up over hills. *Journal of Wind Engineering & Industrial Aerodynamics*, 95, 639–661. https://doi.org/10.1016/j.jweia.2006.09.001

Narjisse, A., & Abdellatif, K. (2021). Assessment of RANS turbulence closure models for predicting airflow in neutral ABL over hilly terrain. *International Review of Applied Sciences and Engineering*, 12(3), 238–256. https://doi.org/10.1556/1848.2021.00264

Norris, S. E., & Richards, P. J. (2010). Appropriate boundary conditions for computational wind engineering models revisited. *The Fifth International Symposium on Computational Wind Engineering (CWE2010)*.

Parente, A., Gorlé, C., Van Beeck, J., & Benocci, C. (2011). Improved k – epsilon model and wall function formulation for the RANS simulation of ABL flows. *Journal of Wind Engineering & Industrial Aerodynamics*, 99, 267–278. https://doi.org/10.1016/j.jweia.2010.12.017

Parente, A., Gorlé, C., Benocci, C., & Dynamics, F. (2010, 23-27 May). *RANS Simulation of ABL Flows : Implementation of Advanced Boundary Conditions for Mixed Rough and Smooth Surfaces RANS Simulation of ABL Flows : Implementation of Advanced Boundary Conditions for Mixed Rough and Smooth Surfaces*. The Fifth International Symposium on Computaional Wind Engineering (CWE 2010).

Parente, A., Longo, R., Ferrarotti, M., & Milano, P. (2017). *CFD boundary conditions , turbulence models and dispersion study for flows around obstacles*. Université Libre de Bruxelles. https://doi.org/10.35294/ls201701.parente

Pontiggia, M., Derudi, M., Busini, V., & Rota, R. (2009). Hazardous gas dispersion: A CFD model accounting for atmospheric stability classes. *Journal of Hazardous Materials*, 171(1–3), 739–747. https://doi.org/10.1016/j.jhazmat.2009.06.064

Richards, P. J., & Hoxey, R. P. (1993). Appropriate boundary conditions for computational wind engineering models using the k-ε turbulence model. *Journal of Wind Engineering and Industrial Aerodynamics*, 46–47(C), 145–153. https://doi.org/10.1016/0167-6105(93)90124-7

Singh, N. K., & Badodkar, D. N. (2016). Modeling and analysis of hydraulic dashpot for impact free operation in a shut-off rod drive mechanism. *Engineering Science and Technology, an International Journal*, 19(3), 1514–1525. https://doi.org/10.1016/j.jestch.2016.05.005

Sørensen, N. N., Bechmann, A., Johansen, J., Myllerup, L., Botha, P., Vinther, S., & Nielsen, B. S. (2007). Identification of severe wind conditions using a Reynolds Averaged Navier-Stokes solver. *Journal of Physics: Conference Series*, 75(1). https://doi.org/10.1088/1742-6596/75/1/012053

Tian, L., Zhao, N., Wang, T., Zhu, W., & Shen, W. (2018). Assessment of in flow boundary conditions for RANS simulations of neutral ABL and wind turbine wake flow. *Journal of Wind Engineering &*

Industrial Aerodynamics, 179 (September 2017), 215–228. https://doi.org/10.1016/j.jweia.2018.06.003

Tian, L., Zhu, C., Zhu, W., & Zhao, N. (2017). Assessment of inflow boundary conditions for RANS simulations of neutral ABL and wind turbine wake flow. *Journal of Wind Engineering and Industrial Aerodynamics*, 179(July), 1–26. https://doi.org/10.20944/preprints201707.0085.v1

Yan, B. W., Li, Q. S., He, Y. C., & Chan, P. W. (2015). RANS simulation of neutral atmospheric boundary layer flows over complex terrain by proper imposition of boundary conditions and modification on the k-e model. *Journal of Environnement Fluid Mechanics*, 16, 1–23. https://doi.org/10.1007/s10652-015-9408-1

Yang, Q., Zhou, T., Yan, B., Liu, M., Van Phuc, P., & Shu, Z. (2021). LES study of topographical effects of simplified 3D hills with different slopes on ABL flows considering terrain exposure conditions. *Journal of Wind Engineering and Industrial Aerodynamics*, 210, 104513. https://doi.org/10.1016/j.jweia.2020.104513

Yang, W., Quan, Y., Jin, X., Tamura, Y., & Gu, M. (2008). *Influences of equilibrium atmosphere boundary layer and turbulence parameter on wind loads of low-rise buildings*. 96, 2080–2092. https://doi.org/10.1016/j.jweia.2008.02.014

Yang, Y., Gu, M., Chen, S., & Jin, X. (2009). New inflow boundary conditions for modelling the neutral equilibrium atmospheric boundary layer in computational wind engineering. *Journal of Wind Engineering and Industrial Aerodynamics*, 97(2), 88–95. https://doi.org/10.1016/J.JWEIA.2008.12.001

Yang, Y., Xie, Z., & Gu, M. (2017). Consistent inflow boundary conditions for modelling the neutral equilibrium atmospheric boundary layer for the SST k-ω model. *Wind and Structures*, 24(5), 465–480. https://doi.org/10.12989/was.2017.24.5.465

Zheng, K. & Tian, W. (2018, January 1–10). *An Experimental Study on the Turbulent Flow Over Two- Dimensional Plateau*s. 2018 Wind Energy Symposium. https://doi.org/10.2514/6.2018-0754.